BIOMATERIALS

Hierarchical wrinkling in a confined permeable biogel

10.1126/sciadv.1500608

Mathieu Leocmach,* Mathieu Nespoulous,† Sébastien Manneville, Thomas Gibaud‡

Confined thin surfaces may wrinkle as a result of the growth of excess material. Elasticity or gravity usually sets the wavelength. We explore new selection mechanisms based on hydrodynamics. First, inspired by yoghurt-making processes, we use caseins (a family of milk proteins) as pH-responsive building blocks and the acidulent glucono-δ-lactone to design a porous biogel film immersed in a confined buoyancy-matched viscous medium. Under specific boundary conditions yet without any external stimulus, the biogel film spontaneously wrinkles in cascade. Second, using a combination of titration, rheology, light microscopy, and confocal microscopy, we demonstrate that, during continuous acidification, the gel first shrinks and then swells, inducing wrinkling. Third, taking into account both Darcy flow through the gel and Poiseuille flow in the surrounding solvent, we develop a model that correctly predicts the wrinkling wavelength. Our results should be universal for acid-induced protein gels because they are based on pH-induced charge stabilization/destabilization and therefore could set a benchmark to gain fundamental insights into wrinkled biological tissues, to texture food, or to design surfaces for optical purposes.

INTRODUCTION

A film wrinkles in many ways and for various reasons. An elastic film buckles because of excess area and wrinkles when a substrate hinders buckling. The selection of the preferred wrinkling wavelength is peculiar to the situation and is related to a mismatch of elastic properties between the surface and the substrate (*1*–*6*). In biology, wrinkling-controlled morphogenesis is ubiquitous. Aging and loss of elastic fibers make our skin wrinkle (*6*, *7*). The difference in growth rate between the gut tube and its dorsal anchoring is responsible for the villification of guts (*8*–*10*). Localized cell death in biofilms focuses on mechanical forces and initiates a three-dimensional labyrinth pattern (*11*, *12*). In physics, the last two decades have seen the development of methods used to obtain well-controlled patterns via linear (*4*, *6*, *13*–*16*) or nonlinear wrinkling (*17*–*20*). Such patterns can be triggered by temperature dilation (*4*), swelling (*13*, *14*), or removal of prestrain (*6*).

Yet, benchmark experiments that explore the possibility of wrinkling in confined porous soft materials immersed in a buoyancy-matched viscous medium are in line, not only to develop the field of physics but also to obtain fundamental insights into biologically relevant situations. Indeed, a stability analysis of a film lying on a thin viscous substrate was performed recently (*21*) but remains theoretical because, on a free interface, gravity dominates a viscous substrate. In a biological context, however, thin tissues (for example, epithelium or endothelium) are naturally confined and immersed in a nearly buoyant medium (for example, lymph, blood, or mucus), a practical situation where a thin viscous substrate would set the wrinkling wavelength (*22*). Moreover, most biological films are porous, and little is known about the interplay between permeability and wrinkling (*23*, *24*). The main goal of the present study is therefore threefold: to create a buoyancy-matched material that wrinkles, to unveil the physical origin of observed patterns, and to identify the selection mechanism of the wavelength.

Université de Lyon, Laboratoire de Physique, Éccole Normale Supérieure de Lyon, CNRS UMR 5672, 46 Allée d'Italie, 69364 Lyon Cedex 07, France.
*Present address: Institut Lumière Matière, UMR 5306 Université Claude Bernard Lyon 1, CNRS, Université de Lyon, Villeurbanne 69622, France.
†Present address: Aix-Marseille Université, CNRS, MADIREL UMR 7246, Marseille 13397, France.
‡Corresponding author: E-mail: thomas.gibaud@ens-lyon.fr

Here, we introduce a model of permeable biogels that produce hierarchical wrinkling as a result of the interplay between gelation dynamics and confinement conditions. We used as a biogel a simplified yoghurt obtained by slow acidification of caseins (a family of milk proteins) (*25*–*28*). While still liquid, an aqueous dispersion of caseins is injected into a home-made optical cell that is then sealed. We designed this cell in such a way that casein adhesion to both top and bottom walls is turned off and the gel is only anchored to the remaining four vertical sides of the cell. Although no external stimulus is exerted on the system, we observe the spontaneous formation of a wrinkling pattern (Fig. 1 and videos S1 and S2). This pattern shows unique properties: a primary pattern simultaneously appears throughout the system, with a wavelength λ that is much smaller than the cell width L and does not evolve with time. Furthermore, in this primary pattern, secondary and ternary patterns appear in cascade. Using a combination of titration, rheology, light microscopy, and confocal microscopy, we demonstrate that wrinkles at the millimeter scale result from the spontaneous swelling of the casein network at the micrometer level upon acidification. Finally, we show that the wavelength is selected by a purely viscous mechanism that combines porous Darcy flow and viscous Poiseuille flow. We systematically ensured that this combined model pins down the dynamic origin of the constraints exerted on the gel and nicely predicts the wrinkling wavelength under a wide range of conditions.

RESULTS AND DISCUSSION

Dynamics of the wrinkling process

To form a biogel, we start from an aqueous dispersion of caseins and glucono-δ-lactone (GDL). GDL slowly acidifies the medium and triggers the gelation of caseins (*25*–*28*). While still liquid, this yoghurt-forming suspension is injected into a home-made optical cell (Fig. 1A). The cell is sealed, and no external stimulus is applied during gelation or pattern formation. Both top and bottom walls are coated with acrylamide brushes, effectively turning off casein adhesion such that the gel is only anchored to the remaining four vertical sides of the cell.

We follow the dynamics of pattern formation by light transmission microscopy and confocal microscopy (see Materials and Methods). As shown in Fig. 1B and video S1, we observe the spontaneous formation of a first pattern that appears with a characteristic wavelength $\lambda \ll L$. The two-dimensional shape and size of this primary pattern are set as soon as the pattern forms and do not evolve with time. However, inside the primary pattern, a secondary pattern emerges, inside which a ternary pattern forms. At each step of this Russian dolls–like cascade, the wavelength is divided by two (fig. S1).

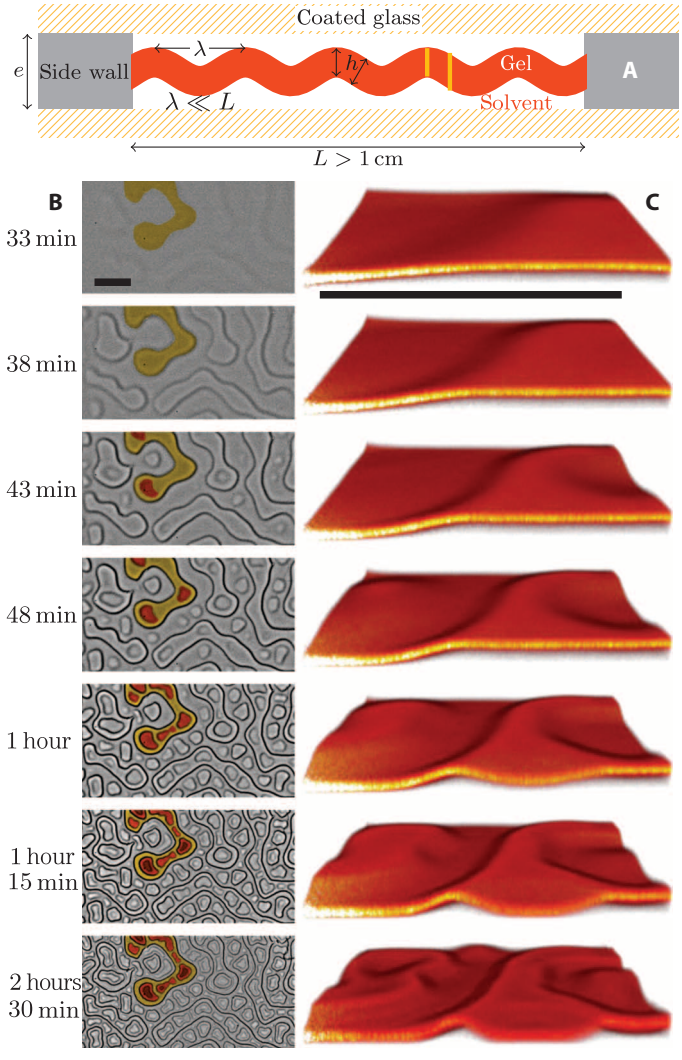

Fig. 1. Dynamics of pattern formation in a confined film of casein gel (4 wt % caseinate and 4 wt % GDL in water). (**A**) Sketch of the cell where adhesion to both top and bottom walls is turned off. The cell is sealed, and the gel is only anchored to the four sides. Typical dimensions are $L > 1$ cm and $e \approx 100$ μm. (**B**) Light transmission microscopy. Successive generations of patterns are highlighted in color to stress the absence of coarsening after formation. The successive wavelengths are $\lambda = 1.5$ mm (yellow), $\lambda = 0.75$ mm (orange), and $\lambda = 0.32$ mm (brown). (**C**) Three-dimensional reconstruction from fluorescent confocal microscopy, which highlights that the patterns observed in (B) correspond to wrinkles. The contrast in (B) is not due to thickness inhomogeneities but is due to altitude gradients, as indicated by yellow vertical lines in (A). Scale bars, 1 mm.

Three-dimensional confocal microscopy (Fig. 1C and video S2) reveals that these patterns actually correspond to wrinkles of the biogel film. Figure 2A shows successive side views of the same confocal measurements as in Fig. 1C (videos S3 and S4). Initially, the dispersion is homogeneous and fills the entire slit. The black margins in Fig. 2A correspond to the glass walls. At around 23 min, the gel forms and simultaneously becomes thinner and more concentrated—the fluorescence signal that is proportional to the casein concentration is brighter than the initial situation. This effect is the fingerprint of syneresis: as gelation proceeds, solvent is expelled through both the upper side and the lower side of the gel film.

Extracting the top and bottom surfaces of the gel phase allows for quantitative measurements of the relative volume (Fig. 2B) and excess surface area of the gel film (Fig. 2C and Supplementary Materials). The evolution of gel volume is surprisingly nonmonotonic. After reaching the minimum (around 35% of its initial value) at 23 min, the volume increases. Shortly

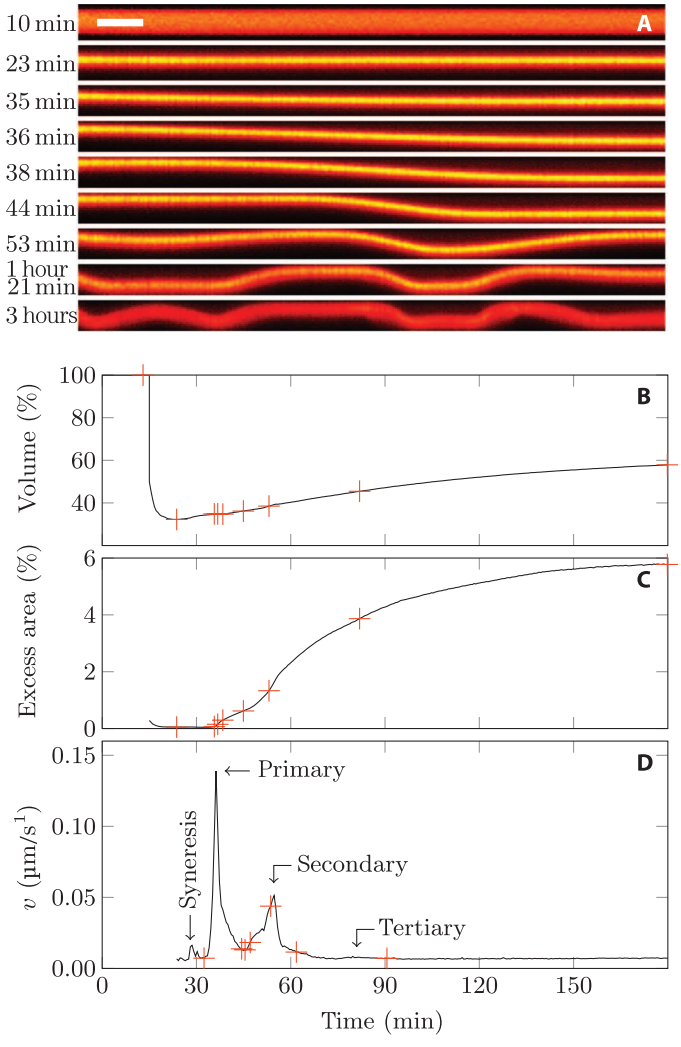

Fig. 2. Three-dimensional analysis of the wrinkling process. (**A**) Confocal (x, z) cuts showing syneresis, swelling, wrinkling, and cascade buckling. Scale bar, 100 μm (real size ratio). (**B** to **D**) Confocal microscopy measurements of the evolution of the volume of the gel phase relative to cell volume, excess area, and velocity along the z-direction. Crosses correspond to times in (A).

after, at 36 min, the planar film destabilizes and starts to wrinkle in the *z*-direction, creating an excess area. This confirms that the instability that leads to the primary pattern is due to swelling. At around 38 min, the amplitude of the wrinkles reaches the thickness of the slit. As swelling continues, the gel flattens on both top and bottom walls (44 min) and finally buckles back (53 min) to form the secondary pattern (1 hour 21 min). When the excess area saturates, the dynamics stop (3 hours). At any given point in time, the thickness h of the gel film is spatially homogeneous.

The primary, secondary, and tertiary patterns follow the same path: the birth of an instability of wavelength λ of growing amplitude $A(t)$ until saturation to A_{max} (Fig. 2A). Throughout the whole process, λ remains constant. This path is dynamic in essence. In Fig. 2D, we thus report the velocity $v(t)$ of the wrinkles as it develops in the *z*-direction (see Supplementary Materials for the definition). We observe that the velocity peaks at different times corresponding to syneresis and to the respective growths of the primary, secondary, and tertiary patterns. We associate each growth with a characteristic time $\tau = A_{max}/v_{max}$. For example, in the present case, the τ value corresponding to the primary pattern is 123 s.

Therefore, contrary to observations by, for example, Yoo and Lee (*29*), we do not report any coarsening of the patterns. We believe that the wrinkling pattern is stable against coarsening because of the bending rigidity of the gel (*30*). Indeed, when the amplitude saturates, the gel flattens against the walls, creating sharp edges. To accommodate those sharp edges with finite bending rigidity, the flat part of the gel actually ripples (fig. S2). The ripples created by the opposite sides of the same flat patch interfere, creating barriers against coarsening (*30*).

On the basis of these observations, we examine possible scenarios upon shrinking and swelling of the gel. As the gel forms, it expels the solvent and detaches from the top and bottom walls (Fig. 3, B and C). For the swelling-back mechanism, we consider three options.

(i) In Fig. 3D, the swelling-back mechanism is reversible, only releasing tensile stresses accumulated during shrinking, and the layer remains flat, as expected of chemical gels (*14*). Because we do not observe this case, it means that, in this physical gel, syneresis and swelling foster irreversible stress dissipation and structural changes. In (ii) and (iii), we will therefore consider the shrunk state to be stress-free.

(ii) In Fig. 3E, we assume that nothing hinders the buckling of the gel film. This simple buckling situation leads to a primary pattern composed of a single bump of size L. As the bump amplitude grows larger and saturates on the top and bottom walls, buckling of smaller wavelength may appear, as observed by Roman and Pocheau (*31*). We do not observe this because our primary wavelength λ is much smaller than L.

(iii) We are left with the case of Fig. 3F, where a wrinkling pattern spontaneously emerges with a wavelength $\lambda \ll L$ selected before saturation on the top and bottom walls. To obtain such instability, one must balance the bending rigidity of the gel film with a transverse load $\sigma_\perp$ that hinders buckling at large wavelengths. The transverse load could be due to gravity (*32*–*36*); however, we confirmed that gravity plays no significant role by successfully repeating the wrinkling pattern in a cell held vertically (that is, with the weight acting longitudinally rather than transversely). Furthermore, the transverse load cannot be adhesion (*37*) because the film does not adhere to the top and bottom walls. The binding of a longitudinal edge to a rigid substrate can induce wrinkles upon compression (*16*, *38*). However, in that case, the wavelength gets larger away from the bound edge. Because the wavelength of our pattern is uniform throughout the sample, we exclude the influence of the side boundaries. Finally, as the four side boundaries remain fixed, $\sigma_\perp$ cannot come from the resistance to uniaxial stretching (*5*).

Therefore, at this stage, our observations raise two unresolved issues that we address in the following sections: (i) What triggers a spontaneous syneresis–swelling-back mechanism? (ii) What is the nature of $\sigma_\perp$, which is responsible for the selection of the primary wavelength?

Syneresis–swelling-back mechanism

The syneresis–swelling-back mechanism depends on the following: (i) pH sensitivity of caseins, (ii) route to gelation, (iii) gel properties, and (iv) boundary conditions.

The stability of casein dispersions strongly depends on pH. Video S5 shows the titration of a casein dispersion (4 wt %) by 1 M HCl. At pH 7,

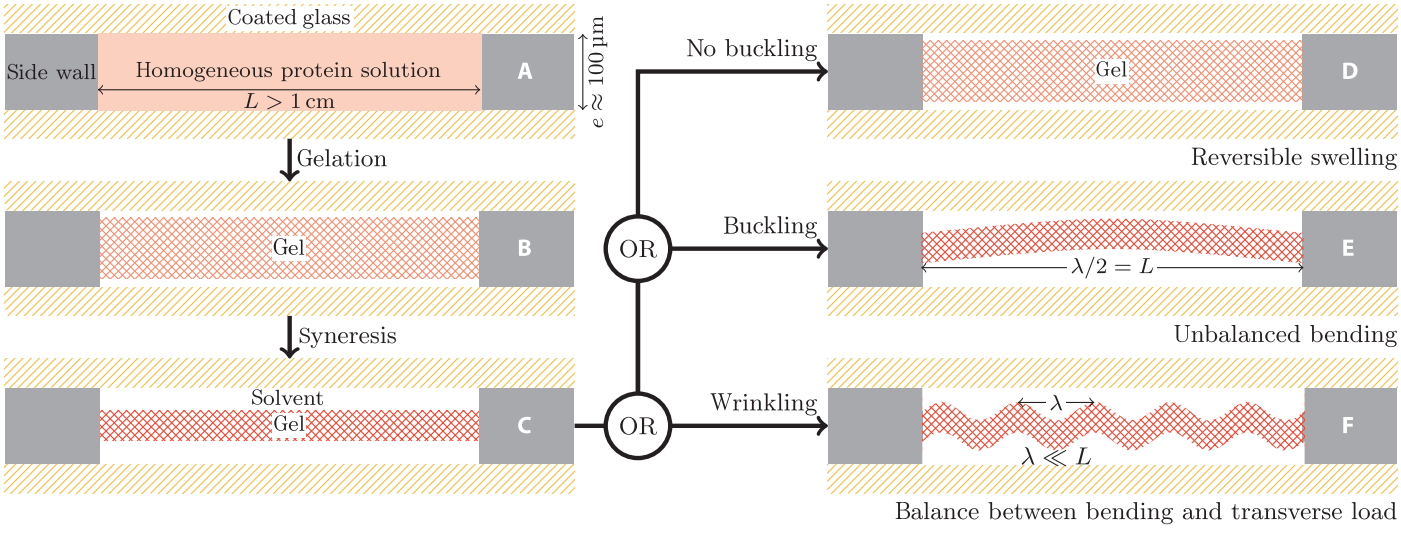

Fig. 3. The wrinkling experiment. (**A**) Initial configuration where the sealed cell contains a homogeneous protein solution. (**B**) Around the isoelectric pH, the gel forms and immediately expels the solvent, leading to (**C**). If tensile stresses were not released, a reversible swelling-back mechanism would occur, leading to (**D**), a flat swollen gel layer. If tensile stresses were released, the swelling-back mechanism would lead either to buckling (**E**) or to wrinkling (**F**), depending on whether bending is free or hindered by a transverse load.

caseins are well dispersed and flocculate between pH 5.5 and pH 4; finally, at pH 3, the solution becomes clearer as caseins partially redisperse. The state diagram of caseins as a function of pH is thus related to charge stabilization. At neutral pH, caseins are charged negatively and repel one another. As pH decreases to the isoelectric point of caseins (pH ≈ 4.6), casein molecules lose their negative net charge and tend to stick to one another (*25*–*28*). Beyond the isoelectric point, caseins acquire a positive net charge and therefore partially redissolve. In Fig. 4B (inset), we quantify this effect and measure, using UV absorption spectroscopy, the amount of free caseins within the 4 wt % dispersion as a function of pH (Supplementary Materials). Starting at pH 6.8, all casein molecules are well dispersed, and the fraction of free caseins x_{free} is 1. As pH decreases toward the isoelectric point, the fraction of free caseins drops to almost 0: almost all of the casein molecules are aggregated.

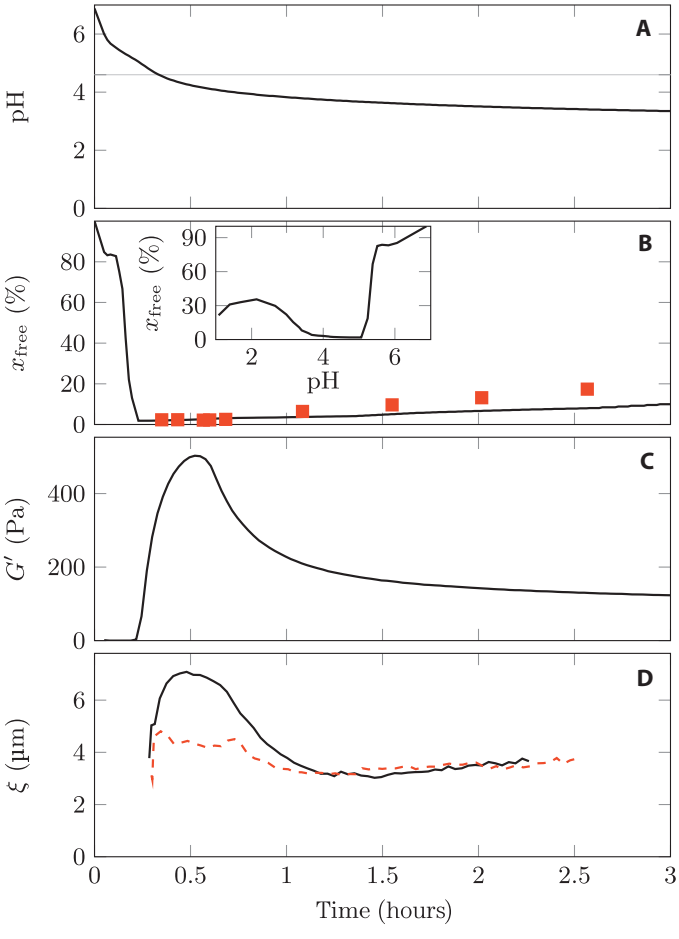

Fig. 4. Acid-induced protein gel properties behave nonmonotonically with pH. (**A**) pH decreases over time in a 4 wt % sodium caseinate solution acidified by 4 wt % GDL in water. The horizontal line indicates the isoelectric pH of caseins. (**B**) Corresponding evolution of the fraction of free caseins. Symbols are direct measures upon addition of GDL. The continuous line is deduced from x_{free} at the same pH obtained by addition of 1 M HCl and upon waiting for equilibration (inset). (**C**) Evolution of the elastic modulus *G*′ measured in a rheometer with full adhesion to the cone-plane geometry. (**D**) Evolution of pore size measured by confocal microscopy in a slit geometry with either adhesion to all walls (black line) or no adhesion to the top wall [that is, allowed syneresis and swelling (orange dashed line)].

A further decrease in the pH of the solution leads to a partial redissolution of casein aggregates. At pH 2, the fraction of free caseins is 0.35.

When acidified by a strong acid-like HCl, caseins flocculate and do not form a space-spanning gel. Therefore, we use GDL, a molecule that slowly hydrolyzes into gluconic acid and thus slowly, continuously, and homogeneously lowers the pH of the suspension (Fig. 4A). This GDL-controlled acidification enables the formation of a bulk gel phase below pH 5.3 with $x_{free} \approx 0$. This process is kinetically driven by diffusion-limited cluster aggregation (*26*). As shown in Fig. 4 (A and B), when enough GDL is added, the pH decreases beyond the isoelectric point, shifting the balance between attraction and charge repulsion at the casein level such that caseins partially dissociate from the fractal network. This results in the coexistence of a dilute phase ($x_{free} \approx 5$ to 20%) and a dense glassy network, a scenario reminiscent of arrested phase separation (*39*, *40*).

We monitor GDL-induced gelation with a rheometer in cone-plate geometry. As casein strongly adsorbs to surfaces, strain and stress are transmitted well to the casein dispersion; thus, we can measure the elastic and viscous moduli of the casein dispersion as a function of time (Fig. 4C). The mechanical properties of the gel are closely related to the fraction of free caseins. First, the dispersion solidifies, then reaches its maximum elasticity (≈500 Pa) at the isoelectric point and, finally, the elastic modulus decreases to ≈ 100 Pa. This finite value indicates that the sample is still a gel.

To gain further insights into the mechanical properties of the gel, we turn to microstructural observations under confocal microscopy. As shown in videos S6 and S7 and fig. S4, the gel consists in a space-spanning fractal network with a cutoff length scale ξ that corresponds to the maximum pore size (*41*). Permeability α is on the order of 67,000 nm^2 (fig. S5). The fractal model fits the structure at all times, but its parameters vary nonmonotonically during GDL acidification. As shown in Fig. 4D and fig. S4, when the isoelectric point is reached, ξ increases up to a maximum length of 7 μm as a result of solvent expulsion out of the casein network (*27*), similar to viscoelastic phase separation (*42*). This corresponds to a tighter packing of caseins in network strands. Such stiffening of the strands explains the observed increase in elasticity. Beyond the isoelectric point, caseins partially regain solubility and packing in the strands loosens, resulting in weaker, thicker strands and smaller pores as ξ decreases to 4 μm, hence the long-term decrease in the elastic modulus.

The final parameter that is essential to form wrinkled patterns is boundary conditions. To turn off the adsorption of caseins on a surface, we coat the surface with polymer brushes (see Materials and Methods), effectively creating nonadhesive boundary conditions for the gel. When casein adhesion to the upper boundary is turned off, the gel detaches from the top wall. However, the gel does not wrinkle because it remains attached to the bottom wall. In this situation, we can monitor ξ (Fig. 4D). ξ remains mostly constant, and variations manifest themselves at the macroscopic level in the volume occupied by the gel.

Therefore, the syneresis–swelling-back mechanism is related to the charge stabilization of casein proteins as a function of pH. In particular, beyond the isoelectric point, caseins are charged and repel one another, leading to swelling at every scale: proteins get farther apart from one another, strands become larger and longer, and the gel sheet swells. Such a mechanism is only effective in producing wrinkles when the adhesion of caseins to both top and bottom walls is turned off. Consistent with our explanation, the amount of GDL (and thus the final pH reached by the suspension) controls the degree of swelling-back. Thus, at low GDL concentrations, we only observe the primary pattern, whereas at high GDL concentrations, we observe the formation of higher-order patterns.

Wavelength selection mechanism

The determination of the characteristic length λ of a wrinkling pattern is an old problem. Large deformations of thin sheets are governed by Föppl–von Kármán equations (*43*), which are essentially impossible to solve in analytical form. However, using scaling and asymptotic arguments, one can obtain the dominant wavelength of the wrinkling pattern up to dimensionless prefactors and isolate the physically meaningful ingredients (*5*, *44*). An elastic film buckles as a result of excess area in its boundaries. Wrinkling is a buckling hindered by a substrate: the mismatch of elastic properties between the film and the substrate selects the preferred wrinkling wavelength (*1*, *2*). λ is then set by the competition between the flexural modulus of the film $B = E/(1 - \nu^2)$ (E, Young modulus; ν, Poisson ratio) and a transverse load $\sigma_\perp$. For small deflections of amplitude A, λ scales as (*33*, *34*)

$$\lambda \sim \left(Ah^3 \frac{B}{\sigma_\perp} \right)^{1/4} \quad (1)$$

This framework has been successfully applied to situations where $\sigma_\perp$ comes from the resistance of an elastic substrate (*1*, *2*). Dealing only with (semi)infinite substrates, Biot generalized the elasticity of both the film and the substrate to viscoelasticity (*3*) or poroelasticity (*45*), leading to the selection of time-dependent kinetic wavelength. Furthermore, Eq. 1 remains valid even when $\sigma_\perp$ comes from resistance to uniaxial stretching (*5*), from gravity (*32*–*36*), from capillary forces (*46*), from boundaries (*16*, *38*), or from adhesion (*37*). However, we have excluded these various origins for $\sigma_\perp$ in the discussion around Fig. 3. The only possible explanation left for $\sigma_\perp$ involves hydrodynamic stresses due to the viscous flow of the solvent, either through the porous gel matrix itself or in the surrounding solvent layers.

Accordingly, we consider the two limit scenarios sketched in Fig. 5 that lead to wrinkling patterns. In a first limit, the gel film sits without sticking to the bottom wall of the cell (that is, $H_1 \to 0$) (Fig. 5A and video S3). Creating a two-dimensional blister requires flowing a solvent of viscosity η through the gel of permeability α. The Darcy law (*47*) relates the pressure gradient $(p_2 - p_1)/h$ to the volume flux per unit area $v = \frac{\alpha}{\eta}\frac{p_1 - p_2}{h} = \frac{dA}{dt}$. Identifying $\sigma_\perp = p_2 - p_1$ and injecting this expression into Eq. 1 yields the wavelength of the Darcy mode as

$$\lambda_D \sim h^{1/2}\alpha^{1/4}\Upsilon^{1/4}, \text{ with } \Upsilon = \frac{B\tau}{\eta} \quad (2)$$

where Υ is a dimensionless viscoelastic factor that quantifies the relative stiffness of the film and the solvent at a characteristic time τ.

The opposite limiting case occurs when an impermeable ($\alpha \to 0$) gel film lies in the middle of the cell ($H \equiv H_1 = H_2$; Fig. 5B and video S4). Here, destabilization over a wavelength λ creates a lubrication ($H \ll \lambda$) flow in viscous layers. By symmetry, the transverse load across the gel $\sigma_\perp = p_2 - p_1$ is also the pressure difference over the wavelength. Using a Poiseuille profile for the flow, $\frac{dA}{dt} \sim \sigma_\perp \frac{H^3}{\eta\lambda^2}$ (*48*), and injecting this expression into Eq. 1 yields the wavelength of the Poiseuille mode as

$$\lambda_P \sim (hH)^{1/2}\Upsilon^{1/6} \quad (3)$$

where we recognize the scaling for the wrinkles of an elastic film on a thin ($H \ll \lambda$) elastic substrate (*5*) (where Υ would be the ratio between the flexural modulus of the film and that of the substrate). Indeed, in the lubrication approximation or at low Reynolds numbers, one can consider a viscous film as elastic with an effective Young modulus $3\eta/\tau$ (*3*, *49*).

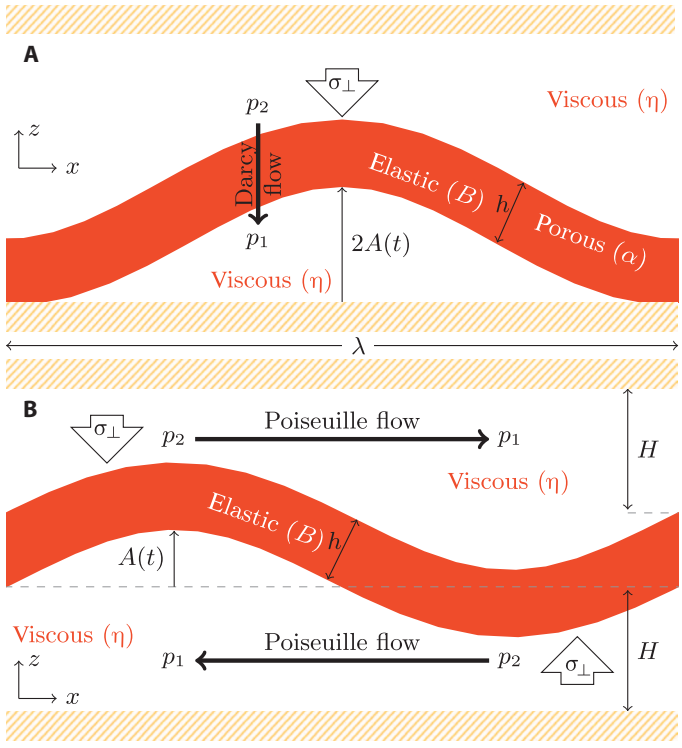

Fig. 5. Sketch of the two limit scenarios for wavelength selection. In both cases, the gel film of thickness h is destabilized by the excess area, which gives rise to wrinkles of amplitude $A(t)$ and wavelength λ. A single wavelength is represented, and the longitudinal dimension L of the system is much larger than λ. The value of λ is set by the interplay between the bending rigidity B and a transverse load $\sigma_\perp$ due to a pressure gradient $p_2 - p_1$ in the solvent of viscosity η. (**A**) Darcy scenario: the gel initially sits without sticking to the bottom wall. $\sigma_\perp$ is due to the flow of the solvent through the porous gel of permeability α to fill the growing blister. (**B**) Poiseuille scenario: the gel film of negligible porosity initially lies in the middle of the cell, separated by a distance H from each wall. $\sigma_\perp$ is due to the lubrication flow in the top and bottom solvent layers.

A more complete derivation of the models can be found in Supplementary Materials and yields the following prefactors

$$\lambda_D = 2\pi h^{1/2}\alpha^{1/4}\left(\frac{\Upsilon}{12}\right)^{1/4} \quad (4)$$

$$\lambda_P = \pi(hH)^{1/2}\left(\frac{2}{9}\Upsilon\right)^{1/6} \quad (5)$$

where H is redefined by $1/H^3 = 1/H_1^3 + 1/H_2^3$. The crossover between the two models where $\lambda_D = \lambda_P$ is found for $H = H^* \equiv 2^{2/3}3^{1/6}\alpha^{1/2}\Upsilon^{1/6}$.

The characteristic time τ is the hallmark of the kinetic nature of wavelength selection mechanisms and is present in the expressions of both λ_D and λ_P.

To sum up, we expect two regimes of viscosity-dominated wrinkling: for $H \ll H^*$ (that is, slow destabilization of a highly permeable film close

to a wall), the main dissipation mechanism is the flow through the porous film; for $H \gg H^*$ (that is, fast wrinkling of a poorly permeable film far from any wall), the flow in viscous layers dominates and sets the wavelength.

Experimental tests

For a typical gel film, we estimate the buoyancy after syneresis from the initial sodium caseinate mass concentration C_{cas} as $\Delta\rho = C_{cas}e/h = 130\ kg/m^3$, leading to a gravity stress $\sigma_\perp^G \approx 0.04$ Pa. This is much lower than typical Darcy or Poiseuille stresses ($\sigma_\perp^D \approx \sigma_\perp^P \approx 0.15$ Pa), confirming that gravity can be neglected, as already inferred from test experiments where the cell is held vertically rather than horizontally.

Darcy and Poiseuille models yield wavelengths that are of the same order in most of the cases under study. Thus, only systematic measurements of experimental λ, together with estimates for all parameters involved in either model, shall allow one to discriminate between them (see Supplementary Materials for such measurements). As summarized in table S1, we systematically vary the following: (i) the thickness of the cell, which affects h and the maximum amplitude; (ii) the gel composition and thus both its stiffness and its permeability; (iii) the viscosity of the solvent (by adding glycerol), which also affects gel stiffness, permeability, and τ. Finally, the only parameter that we have no control over is the initial altitude H of the gel before wrinkling, which varies randomly.

For each experiment, we independently measure λ and all of the parameters that go into the expressions of λ_D (Eq. 4) and λ_P (Eq. 5). We measure λ by optical microscopy; e, h, H_1, H_2, and τ by confocal microscopy; α by capillary rise experiment; and B by rheology (see Materials and Methods and Supplementary Materials).

The beauty of this approach is that modeling the primary wavelength not only is valid but also describes the growth of the secondary pattern. Although the wavelength λ_2 of the secondary pattern is fully determined by the primary pattern $\lambda_2 = \lambda_1/2$ (Fig. 1 and fig. S1), the secondary pattern has its own dynamics with its own characteristic time $\tau_2 \neq \tau_1$. Because the saturation of the primary pattern flattens the gel on the top and bottom walls, the secondary blisters always appear in a Darcy situation ($H \ll H^*$). Therefore, we are able to obtain more data at small H/H^* ratios by considering not only the primary patterns but also the secondary patterns.

Despite changing the gel properties and the cell geometry, we always observe wrinkling, proving the robustness of this approach in forming wrinkling patterns. We are in the position to vary H/H^* from 0.1 to 10 such that we can test the crossover between the Darcy mechanism and the Poiseuille mechanism. In Fig. 6 (A and B), we plot the measured wavelength as a function of the model prediction λ_D and λ_P, respectively. If the predictions are correct, we expect $\lambda_{exp} = \lambda_D$ when $H < H^*$ and $\lambda_{exp} = \lambda_P$ when $H > H^*$. Indeed, both models seem to apply in their domain of validity. The failure of the Poiseuille model is only visible at small wavelengths, where an unexplained offset (Fig. 6B, dashed line) is necessary to correctly fit the data. We further derive a complete model by summing up the influence of both Poiseuille dissipation and Darcy dissipation (Supplementary Materials). The results of this mixed model are displayed in Fig. 6C and agree with λ_{exp} over the whole H/H^* range.

Despite very close agreement on scaling, the exact prefactors of all models disagree by a factor of 0.63 to 0.69. This discrepancy comes from the fact that our model is two-dimensional (that is, uniaxial compression and deflection) whereas our system is three-dimensional (that is, biaxial compression and deflection). Because our system is isotropic in the horizontal plane, this does not change the scaling but could account for a dimensional factor.

CONCLUSION

We took advantage of the properties of casein proteins to engineer and study the wrinkling of a porous confined biogel. In particular, we fine-tuned the interplay between attraction and repulsion at the protein level to assemble dense glassy networks that shrink and swell as a result of continuous acidification. Together with a carefully controlled adhesion of the gels to the boundaries, this route to forming permeable biogels is the key to producing an original cascade of wrinkling patterns. We developed a model that captures the dynamic origin of the constraints exerted on the gel and predicts the wrinkling wavelength: Poiseuille flow of the solvent above and below the gel when the film is far from any wall and Darcy flow of the solvent through the gel when the film is close to a wall. Because the said model experiment relies on pH-induced charge

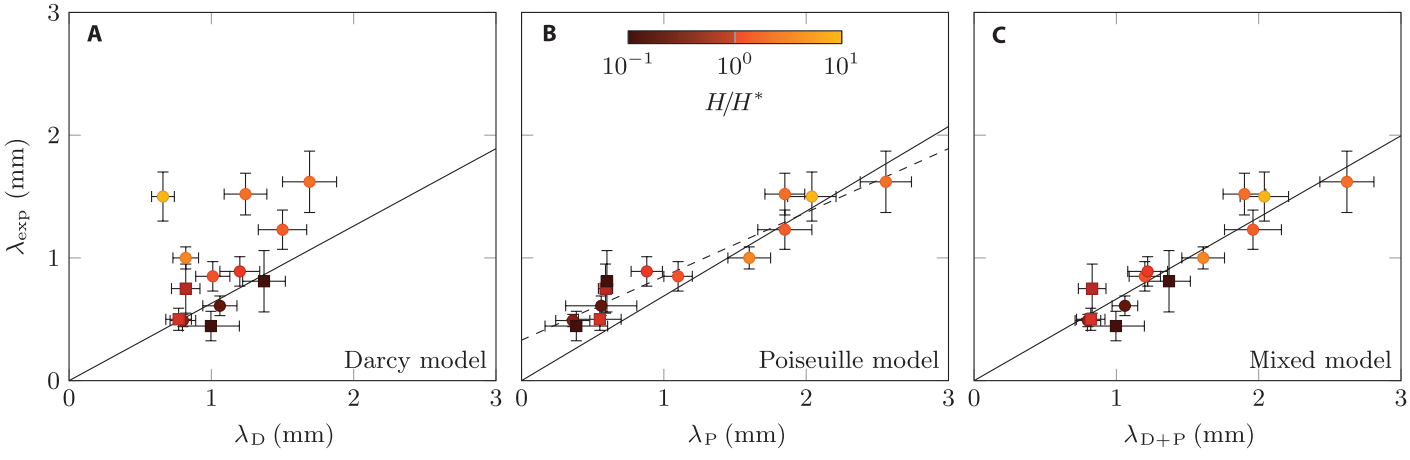

Fig. 6. Comparing model predictions λ_D, λ_P, and λ_{D+P} with measured wavelengths λ_{exp}. Dots, primary pattern; squares, secondary blisters. Lines are the best linear fits through the origin, taking into account (**A**) only the points that should be in Darcy mode $H < H^*$, (**B**) only the points that should be in Poiseuille mode $H > H^*$, and (**C**) all points. The prefactors are 0.63, 0.69, and 0.67 respectively. The dashed line in (B) is the best affine fit ($\lambda_{exp} = 0.52\lambda_P + 0.33$ mm) to all data points.

stabilization/destabilization, it should be generalizable to different kinds of proteins. As such, it could set a benchmark to explore potential applications in microfingerprinting (*50*) or soft optical devices (such as diffraction gratings or Fresnel lenses) (*16*), to texture food (*51*, *52*), and to gain fundamental insights into wrinkling in confined porous soft materials immersed in a buoyancy-matched viscous medium (such as biological tissues) (*22*–*24*).

MATERIALS AND METHODS

We dissolved sodium caseinate (Firmenich) in deionized water by stirring for 20 min at room temperature. Mixing of the casein dispersion with GDL in powder (Firmenich) set the beginning of the experiments. We typically had about 10 min to pipette the dispersion into the slit before gelation starts. We labeled sodium caseinate (Firmenich) with Dylight 550 NHS ESTER (Thermo Scientific). Excess dye was removed by centrifugation. For confocal microscopy measurements, we added 10% of fluorescently labeled caseins to the casein-GDL dispersion while it was still liquid.

Home-made optical cells were composed of a slide (RS) and a cover slip (Menzel-Gläser) spaced by a paraffin film (Parafilm). We briefly heated the optical cell on a hot plate such that the paraffin welded to the slide and to the cover slip. We tuned the thickness of the cell from 50 to 150 μm by gently applying pressure on the cover slip during heating. We filled the slit with the casein dispersion, immediately sealed it with ultraviolet-cured glue (Norland Optical), and placed it under a microscope before gelation took place. To prevent the adsorption of caseins onto surfaces, we cleaned the microscope slides and cover slips used to make microscopy cells and subsequently coated them with a silane agent, 3-(trimethoxysilyl) propyl methacrylate (Sigma Aldrich), from which we polymerized a polyacrylamide brush from methacrylate groups (Euromedex).

We collected three-dimensional data on a Zeiss LSM510 confocal microscope using a laser excitation of 532 nm . We used either a 10× (air) lens to measure the geometry of wrinkling (Supplementary Materials) or a 63× (oil) lens to observe the microstructure of the gel. We used larger-scope pictures, obtained either by stitching fluorescent microscopy (Nikon Eclipse Ti) or by transmitted/reflected light macroscopy (Nikon SMZ745T/Leica DMS1000), to measure the wavelength of the primary pattern (figs. S1 and S3). We took the wavelength of the secondary pattern as being half that of the primary pattern, in accordance with fig. S1. The data shown in Fig. 4A were obtained using a SevenCompact pH meter (Mettler Toledo) and an MCR 301 rheometer (Anton Paar). For every gel composition, we monitored the gelation by small-amplitude oscillations (strain, 0.1%; frequency, 1 Hz) and estimated the flexural modulus B from the maximum value of the shear modulus G' as $B = 2G'/(1 - \nu)$, where $\nu = 0.3$ for the Poisson ratio, a value typical of a spongy network (*53*). We measured permeability following a protocol found in the work of van Dijk and Walstra (*41*) (Supplementary Materials and fig. S5). We measured the amount of free casein proteins present in the gel during GDL acidification by titration and UV spectrometry (Ocean Optics) according to the protocol found in the work of Roefs(*25*) and detailed in Supplementary Materials.

SUPPLEMENTARY MATERIALS

Supplementary material for this article is available at http://advances.sciencemag.org/cgi/content/full/1/9/e1500608/DC1

Fig. S1. Fourier spectra of the binary altitudes of Fig. 1A corresponding to the primary, secondary, and tertiary patterns.

Wavelength measurements

Processing of confocal images

Characteristic time measurements

Fig. S2. Evidence for the ripples generated by the junction to flat patches (*30*).

Fraction of free caseins as a function of pH

Microstructure measurements

Fig. S3. Patterns corresponding to the samples in table S1.

Fig. S4. Microstructure evolution of a 4 wt % sodium caseinate solution acidified with 4 wt % GDL in water.

Permeability measurements

Mixed Darcy-Poiseuille model

Fig. S5. Permeability measurements.

Fig. S6. Schematic side view of the slit.

Table S1. Characteristics of the samples used in Fig. 6.

Video S1. Transmitted light microscopy images of pattern formation in a casein (4 wt %)–GDL (4 wt %) aqueous dispersion.

Video S2. Three-dimensional reconstruction of pattern formation using confocal microscopy in a casein (4 wt %)–GDL (4 wt %) aqueous dispersion (table S1C).

Video S3. Confocal microscopy (x, z) cut of the evolution of the gel film deflection of a casein (4 wt %)–GDL (4 wt %) aqueous dispersion when both top and bottom walls are coated with acrylamide brushes (table S1A).

Video S4. Confocal microscopy (x, z) cut of the evolution of the gel film deflection of a casein (4 wt %)–GDL (4 wt %) aqueous dispersion when both top and bottom walls are coated with acrylamide brushes (table S1C).

Video S5. Titration of a dispersion with 4 wt % casein by 1 M HCl.

Video S6. Confocal microscopy (x, y) cut of the evolution of the local structure of a casein (4 wt %)–GDL (4 wt %) aqueous dispersion in sticky boundaries.

Video S7. Confocal microscopy (x, y) cut of the evolution of the local structure of a casein (4 wt %)–GDL (4 wt %)aqueous dispersion when the top wall is coated with acrylamide brushes and the bottom wall remains sticky.

REFERENCES AND NOTES

1. C. S. Gough, C. F. Elam, N. A. De Bruyne, The stabilization of a thin sheet by a continuous support medium. *J. R. Aeronaut. Soc.* **44**, 12–43 (1940).
2. P. P. Bijlaard, On the elastic stability of thin plates, supported by a continuous medium. *R. Dutch Acad. Sci. Proc.* **49**, 1189–1199 (1946).
3. M. A. Biot, Folding instability of a layered viscoelastic medium under compression. *Proc. R. Soc. A Math. Phys. Eng. Sci.* **242**, 444–454 (1957).
4. N. Bowden, S. Brittain, A. G. Evans, J. W. Hutchinson, G. M. Whitesides, Spontaneous formation of ordered structures in thin films of metals supported on an elastomeric polymer. *Nature* **393**, 146–149 (1998).
5. E. Cerda, L. Mahadevan, Geometry and physics of wrinkling. *Phys. Rev. Lett.* **90**, 074302 (2003).
6. J. Genzer, J. Groenewold, Soft matter with hard skin: From skin wrinkles to templating and material characterization. *Soft Matter* **2**, 310–323 (2006).
7. D. L. Bissett, D. P. Hannonand, T. V. Orr, An animal model of solar-aged skin: Histological, physical, and visible changes in UV-irradiated hairless mouse skin. *Photochem. Photobiol.* **46**, 367–378 (1987).
8. T. Savin, N. A. Kurpios, A. E. Shyer, P. Florescu, H. Liang, L. Mahadevan, C. J. Tabin, On the growth and form of the gut. *Nature* **476**, 57–62 (2011).
9. P. Ciarletta, V. Balbi, E. Kuhl, Pattern selection in growing tubular tissues. *Phys. Rev. Lett.* **113**, 248101 (2014).
10. A. E. Shyer, T. Tallinen, N. L. Nerurkar, Z. Wei, E. S. Gil, D. L. Kaplan, C. J. Tabin, L. Mahadevan, Villification: How the gut gets its villi. *Science* **342**, 212–218 (2013).
11. M. Trejo, C. Douarche, V. Bailleux, C. Poulard, S. Mariot, C. Regeard, E. Raspaud, Elasticity and wrinkled morphology of *Bacillus subtilis* pellicles. *Proc. Natl. Acad. Sci. U.S.A.* **110**, 2011–2016 (2013).
12. M. Asally, M. Kittisopikul, P. Rué, Y. Du, Z. Hu, T. Çağatay, A. B. Robinson, H. Lu, J. Garcia-Ojalvod, G. M. Süel, Localized cell death focuses mechanical forces during 3D patterning in a biofilm. *Proc. Natl. Acad. Sci. U.S.A.* **109**, 18891–18896 (2012).
13. Z. Hu, Y. Chen, C. Wang, Y. Zheng, Y. Li, Polymer gels with engineered environmentally responsive surface patterns. *Nature* **393**, 149–152 (1998).
14. J. Kim, J. Yoon, R. C. Hayward, Dynamic display of biomolecular patterns through an elastic creasing instability of stimuli-responsive hydrogels. *Nat. Mater.* **9**, 159–164 (2010).
15. H. Vandeparre, S. Desbief, R. Lazzaroni, C. Gay, P. Damman, Confined wrinkling: Impact on pattern morphology and periodicity. *Soft Matter* **7**, 6878–6882 (2011).
16. R. Li, H. Yi, X. Hu, L. Chen, G. Shi, W. Wang, T. Yang, Generation of diffraction-free optical beams using wrinkled membranes. *Sci. Rep.* **3**, 2775 (2013).

17. K. Efimenko, M. Rackaitis, E. Manias, A. Vaziri, L. Mahadevan, J. Genzer, Nested self-similar wrinkling patterns in skins. *Nat. Mater.* **4**, 293–297 (2005).
18. M. Guvendiren, J. A. Burdick, S. Yang, Solvent induced transition from wrinkles to creases in thin film gels with depth-wise crosslinking gradients. *Soft Matter* **6**, 5795–5801 (2010).
19. P. Kim, M. Abkarian, H. A. Stone, Hierarchical folding of elastic membranes under biaxial compressive stress. *Nat. Mater.* **10**, 952–957 (2011).
20. F. Brau, H. Vandeparre, A. Sabbah, C. Poulard, A. Boudaoud, P. Damman, Multiple-length-scale elastic instability mimics parametric resonance of nonlinear oscillators. *Nat. Phys.* **7**, 56–60 (2011).
21. R. Huang, Z. Suo, Wrinkling of a compressed elastic film on a viscous layer. *J. Appl. Phys.* **91**, 1135–1142 (2002).
22. V. Fleury, N. R. Chevalier, F. Furfaro, J.-L. Duband, Buckling along boundaries of elastic contrast as a mechanism for early vertebrate morphogenesis. *Eur. Phys. J. E* **38**, 92 (2015).
23. F. Ma, E. Cholewa, T. Mohamed, C. A. Peterson, M. Gijzen, Cracks in the palisade cuticle of soybean seed coats correlate with their permeability to water. *Ann. Bot.* **94**, 213–228 (2004).
24. J. E. Longley, L. Mahadevan, M. K. Chaudhury, How a blister heals. *Europhys. Lett.* **104**, 46002 (2013).
25. S. P. Roefs, Structure of acid casein gels: A study of gels formed after acidification in the cold, thesis, Wageningen Agricultural University (1986).
26. L. G. B. Bremer, T. van Vliet, P. Walstra, Theoretical and experimental study of the fractal nature of the structure of casein gels. *J. Chem. Soc. Faraday Trans. 1* **85**, 3359–3372 (1989).
27. J. A. Lucey, H. Singh, Formation and physical properties of acid milk gels: A review. *Food Res. Int.* **30**, 529–542 (1997).
28. E. Dickinson, L. M. Merino, Effect of sugars on the rheological properties of acid caseinate-stabilized emulsion gels. *Food Hydrocolloids* **16**, 321–331 (2002).
29. P. J. Yoo, H. H. Lee, Evolution of a stress-driven pattern in thin bilayer films: Spinodal wrinkling. *Phys. Rev. Lett.* **91**, 154502 (2003).
30. T. Le Goff, P. Politi, O. Pierre-Louis, Frozen states and order-disorder transition in the dynamics of confined membranes. *Phys. Rev. E* **90**, 032114 (2014).
31. B. Roman, A. Pocheau, Buckling cascade of thin plates: Forms, constraints and similarity. *Europhys. Lett.* **46**, 602 (1999).
32. M. Smoluchowski, Versuche über Faltungserscheinungen schwimmender elastischer Platten. *Akad. Wiss. Krakau. Math. Kl.* **2**, 227 (1910).
33. J. M. Kolinski, P. Aussillous, L. Mahadevan, Shape and motion of a ruck in a rug. *Phys. Rev. Lett.* **103**, 174302 (2009).
34. D. Vella, A. Boudaoud, M. Adda-Bedia, Statics and inertial dynamics of a ruck in a rug. *Phys. Rev. Lett.* **103**, 174301 (2009).
35. M. Piñeirua, N. Tanaka, B. Roman, J. Bico, Capillary buckling of a floating annulus. *Soft Matter* **9**, 10985–10992 (2013).
36. A. Lucantonio, M. Roché, P. Nardinocchi, H. A. Stone, Buckling dynamics of a solvent-stimulated stretched elastomeric sheet. *Soft Matter* **10**, 2800–2804 (2014).
37. D. Vella, J. Bico, A. Boudaoud, B. Roman, P. M. Reis, The macroscopic delamination of thin films from elastic substrates. *Proc. Natl. Acad. Sci. U.S.A.* **106**, 10901–10906 (2009).
38. H. Vandeparre, M. Piñeirua, F. Brau, B. Roman, J. Bico, C. Gay, W. Bao, C. N. Lau, P. M. Reis, P. Damman, Wrinkling hierarchy in constrained thin sheets from suspended graphene to curtains. *Phys. Rev. Lett.* **106**, 224301 (2011).
39. F. Cardinaux, T. Gibaud, A. Stradner, P. Schurtenberger, Interplay between spinodal decomposition and glass formation in proteins exhibiting short-range attractions. *Phys. Rev. Lett.* **99**, 118301 (2007).
40. P. J. Lu, E. Zaccarelli, F. Ciulla, A. B. Schofield, F. Sciortino, D. A. Weitz, Gelation of particles with short-range attraction. *Nature* **453**, 499–503 (2008).
41. H. J. M. van Dijk, P. Walstra, Syneresis of curd. 2. One-dimensional syneresis of rennet curd in constant conditions. *Netherl. Milk Dairy J.* **40**, 3–30 (1986).
42. H. Tanaka, Viscoelastic phase separation. *J. Phys. Condens. Matter* **12**, R207–R264 (2000).
43. L. D. Landau, E. M. Lifchitz, *Course of Theoretical Physics: Theory of Elasticity* (Butterworth-Heinemann, Oxford, UK, ed. 3, 1986).
44. B. Davidovitch, R. D. Schroll, D. Vella, M. Adda-Bedia, E. A. Cerda, Prototypical model for tensional wrinkling in thin sheets. *Proc. Natl. Acad. Sci. U.S.A.* **108**, 18227–18232 (2011).
45. M. A. Biot, Theory of buckling of a porous slab and its thermoelastic analogy. *J. Appl. Mech.* **31**, 194–198 (1964).
46. J. Huang, M. Juszkiewicz, W. H. de Jeu, E. Cerda, T. Emrick, N. Menon, T. P. Russell, Capillary wrinkling of floating thin polymer films. *Science* **317**, 650–653 (2007).
47. H. Darcy, *Les Fontaines Publiques de la Ville de Dijon* (Victor Dalmont, Paris, France, 1856).
48. J. L. M. Poiseuille, Recherches expérimentales sur le mouvement des liquides dans les tubes de très petits diamètres. *C. R. Hebd. Seances Acad. Sci.* **15**, 1167 (1842).
49. A. Boudaoud, S. Chaïeb. Singular thin viscous sheet. *Phys. Rev. E* **64**, 050601 (2001).
50. H. J. Bae, S. Bae, C. Park, S. Han, J. Kim, L. N. Kim, K. Kim, S. H. Song, W. Park, S. Kwon, Biomimetic microfingerprints for anti-counterfeiting strategies. *Adv. Mater.* **27**, 2083–2089 (2015).
51. R. Mezzenga, P. Schurtenberger, A. Burbidge, M. Michel, Understanding foods as soft materials. *Nat. Mater.* **4**, 729–740 (2005).
52. T. Gibaud, N. Mahmoudi, J. Oberdisse, P. Lindner, J. S. Pedersen, C. L. P. Oliveira, A. Stradner, P. Schurtenberger, New routes to food gels and glasses. *Faraday Discuss.* **158**, 267–284 (2012).
53. G. N. Greaves, A. L. Greer, R. S. Lakes, T. Rouxel, Poisson's ratio and modern materials. *Nat. Mater.* **10**, 823–837 (2011).

Acknowledgments: Confocal experiments were conducted at SFR BioSciences Gerland–Lyon Sud (US8/UMS3444). We thank J. Bico, A. Boudaoud, C. Gay, L. Mahadevan, and O. Pierre-Louis for theoretical insights at various stages of the research. Precious experimental ideas came from C. Barentin, D. Bartolo, E. Bouchaud, and T. Divoux. A. Parker (Firmenich) provided the caseins and GDL. Special thanks to Madame Biot who made the work of M.A. Biot accessible through the PoroNet Web site. **Funding:** M.L. thanks the Region Rhoˆne Alpes and the Programme d'Avenir Lyon–Saint Etienne (PALSE NoGELPo) for a postdoctoral grant. T.G. and M.N. acknowledge funding from the Agence Nationale de la Recherche (ANR-11-PDOC-027). S.M. and M.L. acknowledge funding from the European Research Council, under the European Union's Seventh Framework Program (FP7/2007-2013)/ERC grant agreement no. 258803, and funding from Institut Universitaire de France. **Author contributions:** M.L. and M.N. conducted the preliminary experiments. M.L., S.M., and T.G. designed the experiments and interpreted the results. M.L. and T.G. performed the quantitative experiments. M.L. performed data analysis and modeling. M.L., S.M., and T.G. wrote the manuscript. **Competing interests:** The authors declare that they have no competing financial interests. **Data and materials availability:** Requests for materials should be addressed to T.G. (thomas.gibaud@ens-lyon.fr).

Submitted 15 May 2015
Accepted 1 August 2015
Published 16 October 2015
10.1126/sciadv.1500608

Citation: M. Leocmach, M. Nespoulous, S. Manneville, T. Gibaud, Hierarchical wrinkling in a confined permeable biogel. *Sci. Adv.* **1**, e1500608 (2015).

Hierarchical wrinkling in a confined permeable biogel

Mathieu Leocmach, Mathieu Nespoulous, Sébastien Manneville and Thomas Gibaud

Sci Adv **1** (9), e1500608.
DOI: 10.1126/sciadv.1500608